Monolithic Capacitors as Transmission Lines

MARK INGALLS AND GORDON KENT, SENIOR MEMBER, IEEE

Abstract—**The results of network analyzer measurements of high-Q multilayer (monolithic) chip capacitors show that the devices have the characteristics of open-circuited transmission lines. Both standard sizes (MIL-CDR-14 and MIL-CDR-12), ranging in capacitance values from 4.7 to 1000 pF, were tested on microstrip lines. A simple model of a periodically loaded line provides a dispersion relation that accounts for the distribution of resonant frequencies. The orientation of the capacitor with respect to the microstrip affects the occurrence and nature of resonances. This phenomenon is shown to result from a distributed excitation source. The unfolding of the capacitor to produce the periodic line is shown to produce anomalies in the dissipation loss when skin depth and electrode thickness are comparable.**

I. Introduction

AT LOW FREQUENCIES, the monolithic ceramic (porcelain) capacitor illustrated in Fig. 1 can be adequately characterized as an ideal capacitor with a small series resistance and series inductance. The resistance, attributable to the losses in the electrodes, is a function of the skin effect, and it increases slowly with frequency. The series inductance accounts for the change in apparent capacitance with frequency as the first self-resonance is approached. Near and above this resonance, the simple *R-L-C* series circuit fails to account for observed characteristics.

An alternative to the *R-L-C* model of the capacitor is a folded transmission line [1]. The process of folding is equivalent to the periodic loading of a straight parallel-plate line, as indicated in Fig. 2. Although the argument for this model is compromised by the fact that the skin depth is comparable to the electrode thickness over the frequency range 0.5–2.0 GHz, the folded-line model proves successful for the interpretation of a wide range of measurements.

In Section II of this paper, we present typical observed characteristics, selected from data on two styles of capacitors, ranging in nominal value from 4.7 pF to 1000 pF. Section III contains an analysis of transmission models for the capacitors. Comparisons of observed and calculated characteristics are presented in Section IV. Concluding remarks are presented in Section V.

II. Experimental Observations

Insertion loss, return loss, and polar plots have been produced by the Hewlett Packard 8510 and Wiltron 5600 network analyzers. All devices tested were mounted on 50-Ω microstrip transmission lines. Polar plots were made of S_{11} with the capacitor short-circuited on the board. Tests were made with capacitors mounted with the electrodes parallel to the substrate, designated H, and normal to the substrate, designated V. These mountings are illustrated in Fig. 1.

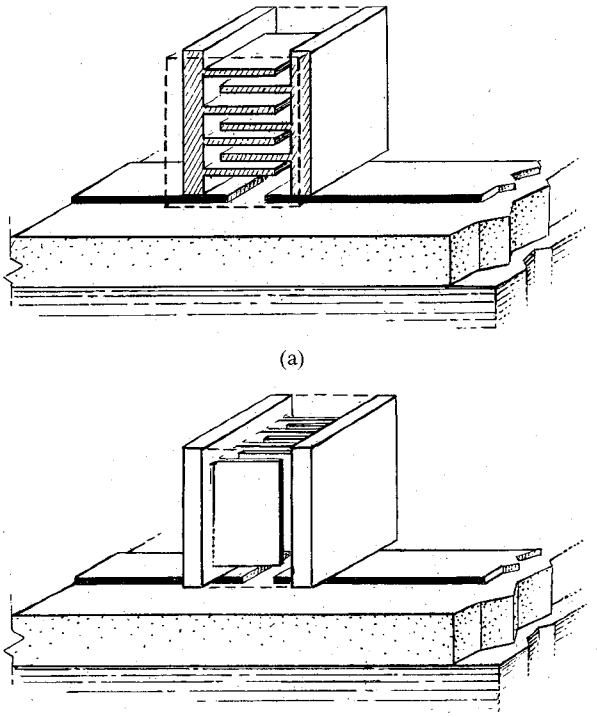

Fig. 1. Monolithic capacitor mounted (a) with internal electrodes horizontal, designated H, and (b) with internal electrodes vertical, designated V. Standard sizes are DL-11 (MIL-CDR-12), approximately 0.05 in on a side, and DL-17 (MIL-CDR-14), approximately 0.11 in on a side.

The capacitors measured were randomly picked within a tolerance category, and the samples varied in number from two to six. Since the spread in those results was very small, only typical data are presented.

All units show both series and parallel resonances. The series resonances are very broad and correspondingly difficult to measure [2]. Although the Q of the capacitor may be high, the loaded Q that one observes is determined by the external Q of the 50-Ω system, and this is normally very low. The definition of series resonance as that frequency at which the capacitor reactance is zero also fails to give precise results. The phase measurement is sensitive to the location of the reference plane and reactances associated with the coupling from the line to the capacitor.

Manuscript received March 11, 1987; revised July 10, 1987.

The authors are with Dielectric Laboratories, Inc., Casenovia, NY 13035.

IEEE Log Number 8716914.

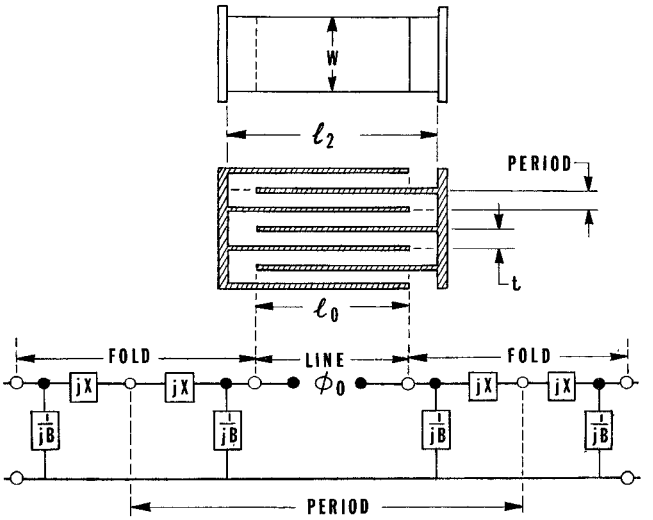

Fig. 2. Cross section of a model capacitor showing (below) the equivalent circuit of one period.

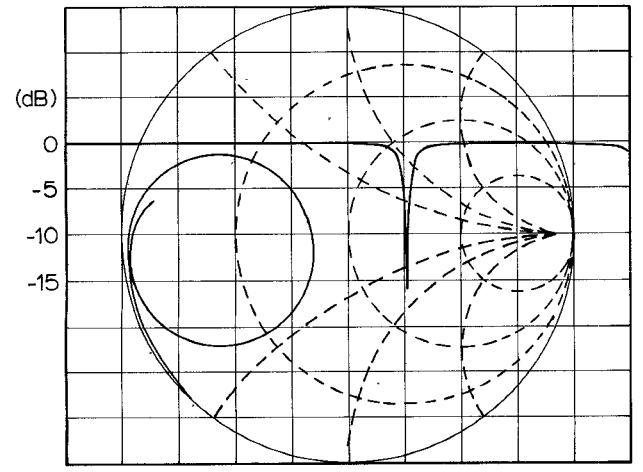

Fig. 3. Sample of graphical data, produced by the HP-8510 network analyzer, that shows typical series and parallel resonance effects. The frequency range is 0.045–2.000 GHz.

The parallel resonances are relatively sharp, and they can be defined and measured as the frequencies of maximum energy absorption. This definition makes the measurement insensitive to fixture mismatch errors.

Fig. 3 illustrates the evidence of series and parallel resonances for a capacitor mounted on a short circuited microstrip line. An error of one or two degrees in determining the phase of S_{11} near 180° corresponds to a substantial error in the series resonant frequency; it also corresponds to a length on the microstrip that may be of the order of the capacitor's dimensions. The parallel resonance is unambiguously shown by the sharp minimum of $\log|S_{11}|$.

Fig. 4 shows the sequence of parallel resonances observed for five DL-17 capacitors. Similar results were found for all sizes and capacitor values. Resonances may occur at frequencies above those shown, but increasing losses tend to obscure the resonance effects. The frequency

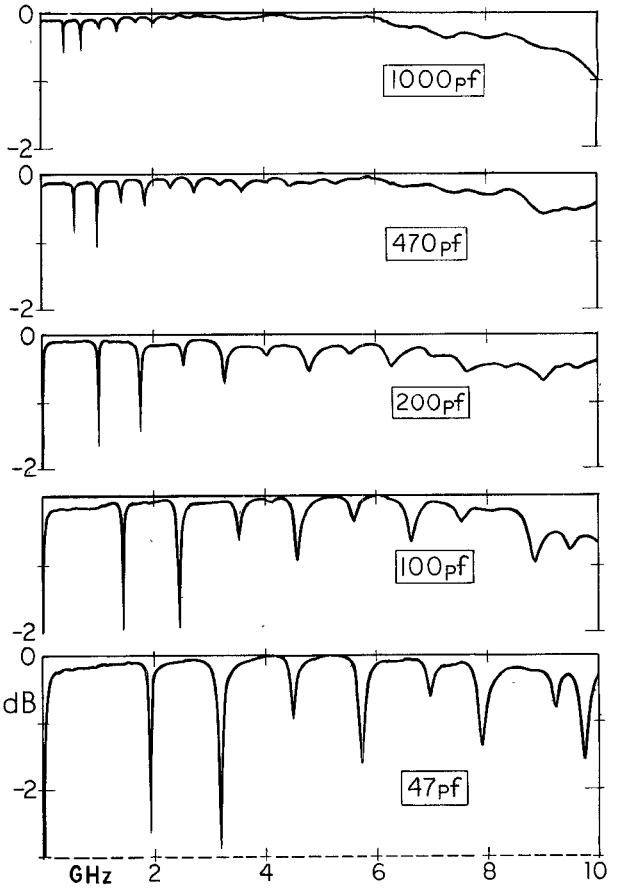

Fig. 4. Insertion loss plots for five DL-17 capacitors.

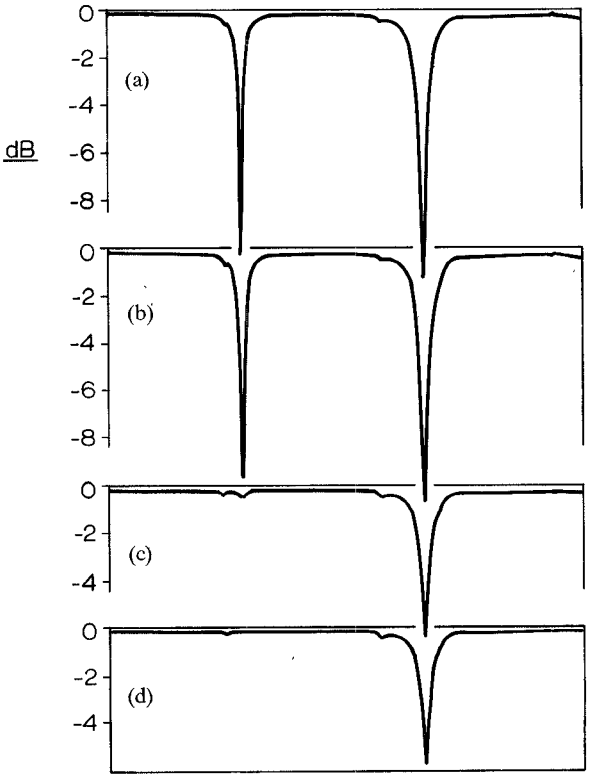

Fig. 5. The effects of asymmetric mounting on observed resonances. (a) H-mounting centered, (b) H-mounting off center, (c) V-mounting off center, and (d) V-mounting centered. The sweep range is 0.05–3.00 GHz.

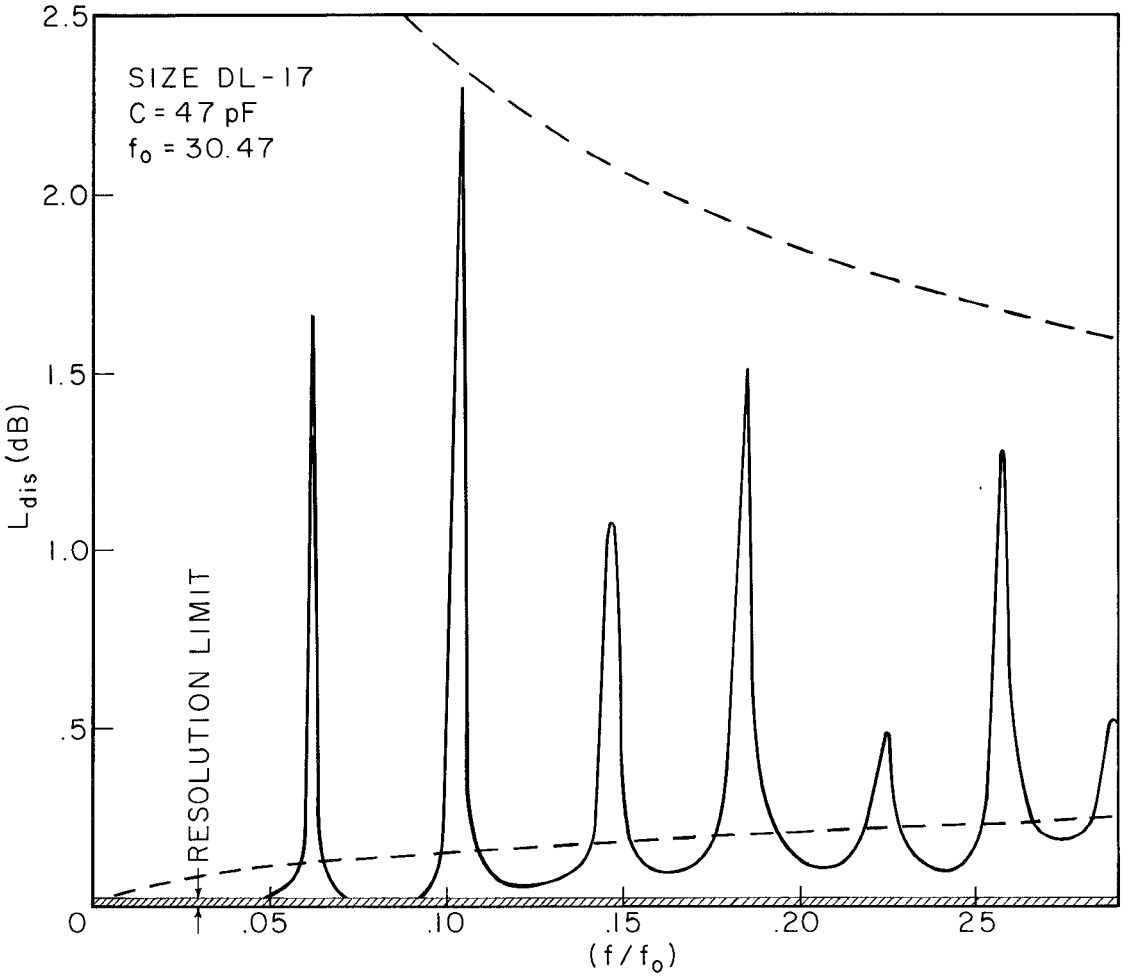

Fig. 6 Typical frequency dependence of dissipation loss. Superposed on the curves plotted from data are envelopes (dashed curves) derived from a uniform line model with losses determined by skin effect

separation of resonances tends to decrease as the frequency increases.

As reported elsewhere [3], the odd-numbered parallel resonances found with the H-mounting are not generally observed with the V-mounting. Phase information, such as that shown in Fig. 3, indicates that the suppressed parallel resonances of the H-mounting become the series resonances of the V-mounting. Complete suppression, however, depends on the location of the capacitor with respect to the center of the microstrip.

Fig. 5 shows the return loss in dB versus frequency of a capacitor (100 pF) mounted on a 25-mil microstrip terminated in a short circuit. For the data of Fig. 5(a), the capacitor is centered in the H-mounting. At the first two parallel resonances, the return loss exceeds 10 dB. No significant change in resonant frequency or return loss occurs when the H-mounting is off center, as shown in Fig. 5(b). The data for the centered V-mounting, Fig. 5(d), show full suppression of the first resonance and a significant reduction of the return loss at the second. When the V-mounting is off center, Fig. 5(c), the first resonance is again evident. Although the effect is very small, this interpretation is justified by the polar plots.

The dissipation loss of a typical unit in the H-mounting is shown in Fig. 6. In the calculations for the figure, the fixture was represented by an equivalent series resistance. The broad minima and sharp maxima show the contrast in definition of the series and parallel resonances. Also a typical feature, the maxima and minima do not lie on smooth envelope curves. To emphasize this characteristic, the envelopes for a uniform open-circuited transmission line with losses determined by skin effect are shown as dashed curves.

The sequence of alternate series and parallel resonances indicates that a transmission line model of the capacitor is more useful than a lumped-element ladder network [4] in which the number of sections would vary from one unit to another. In view of the structure of a capacitor, the folded line or the equivalent periodically loaded line seems most appropriate.

III. Analysis of the Periodically Loaded Line

A. Two-Parameter Representation of the Lossless Line

One can argue the plausibility of representing the fold in the line by a series inductive reactance and a shunt capacitive susceptance. If the element values are independent of

frequency, both reactance and susceptance are strictly proportional to frequency. Thus, the element values are the two parameters to be determined either by calculation or from experimental data. An alternate representation of the fold is a short uniform transmission line of characteristic impedance different from that of the straight, unfolded portion of the line. In this case, the frequency dependence of the reactance and susceptance is sinusoidal, and the two parameters are length and characteristic impedance. At low frequencies, the two representations are equivalent. The limitations of both approaches provide no compelling argument for choosing one above the other, but some analytic simplicity is achieved by using transmission line calculations for both the fold and the nonfolded parts.

For a half-length of fold for which $\phi_1 = (\omega l_1 / v_{ph})$, the reactance and susceptance [5] of Fig. 2 are

$$X = (Z_0/\eta)\sin\phi_1\cos\phi_1 \tag{1}$$

$$B = (\eta/Z_0)\tan\phi_1 \tag{2}$$

where

$$\eta = (Z_0/Z_1) \tag{3}$$

$$Z_0 = (\mu_0/\epsilon)^{1/2}(t/w). \tag{4}$$

The elements of the impedance matrix for the period are found to be

$$Z_{11} = jZ_0\left[\frac{\sin\phi_1\cos\phi_1}{\eta} - \frac{\cos\phi_0 - \eta\tan\phi_1\sin\phi_0}{2\eta\tan\phi_1\cos\phi_0 + (1-\eta^2\tan^2\phi_1)\sin\phi_0}\right] \tag{5}$$

$$Z_{21} = \frac{-jZ_0}{2\eta\tan\phi_1\cos\phi_0 + (1-\eta^2\tan^2\phi_1)\sin\phi_0} \tag{6}$$

where $\phi_0 = (\omega l_0 / v_{ph})$. These impedances are related to the phase shift per period [6], ψ, by

$$\cos\psi = (Z_{11}/Z_{21}) = \cos 2\phi_1\cos\phi_0 - \frac{1+\eta^2}{2\eta}\sin 2\phi_1\sin\phi_0 \tag{7}$$

and the characteristic impedance of the loaded line, Z_c, is

$$Z_c = jZ_{21}\sin\psi. \tag{8}$$

When the capacitor is driven at one end of the folded line and the other end is open or shorted, the driving point impedances are, respectively,

$$Z_{oc} = -jZ_c\cot N\psi \tag{9}$$

$$Z_{sc} = jZ_c\tan N\psi \tag{10}$$

where N is the number of periods.

The parameters η and l_1 for the fold can be related to the dc capacitance C_0 and inductance L_0 by taking limiting values of (9) and (10) and using (7) and (8). The result is

$$l_0 + 2\eta l_1 = (Z_0 v_{ph}/N)C_0 \tag{11}$$

$$l_0 + (2/\eta)l_1 = (v_{ph}/NZ_0)L_0. \tag{12}$$

At least in principle, η and l_1 can be obtained from measurements of C_0 and L_0. The practical problem is that one must disect the capacitor to provide the short for the measurement of L_0.

The limiting values of (11) and (12) are preserved in the approximation of (7),

$$\cos\psi = \cos\phi - (1/\eta - \eta)\phi_1\sin\phi \tag{13}$$

where $\phi = \phi_0 + 2\eta\phi_1$. The coefficient of $\cos\phi$ is accurate to the order ϕ_1^4, and the coefficient of $\sin\phi$ is accurate to order ϕ_1^3. The quantity $2\eta\phi_1$ can be calculated from (11). To the same order of approximation, the characteristic impedance is

$$Z_c = Z_0[1-(1-\eta^2)\phi_1^2][\sin\psi/\sin\phi]. \tag{14}$$

Clearly, (13) and (14) are good approximations at the lower frequencies and for capacitors with a relatively small value of $(l_2 - l_0)$. Moreover, the cutoff frequency that is characteristic of periodically loaded lines is embedded in (13).

B. The Effects of Capacitor Excitation

The periodic line of the capacitor in the H-mounting is driven at one end, and the other end is open; but in the V-mounting, the line is excited over some portion of its interior, and both ends are open. The fields underneath the microstrip are exposed to the edges of the capacitor electrodes through the window formed by the microstrip gap. Although the electric fields that terminate on the electrode edges induce charges, the principal excitation is the current induced by the transverse magnetic field.

To examine the effects of this distributed source, we assume the capacitor to be a uniform line characterized by L, the inductance per meter, and C, the capacitance per meter. With the induced current represented by $J_0(z)$ A/m, the equations for the line voltage and current are

$$dI/dz + j\omega CV = J_0(z) \tag{15}$$

$$dV/dz + j\omega LI = 0. \tag{16}$$

The line extends from $z = 0$ to $z = a$. To solve the line equations, we put

$$V(z) = \sum v_n\cos k_n z \tag{17}$$

$$I(z) = \sum i_n\sin k_n z \tag{18}$$

$$J_0(z) = \sum j_n\cos k_n z \tag{19}$$

where $k_n = (n\pi/a)$, $n = 0,1,\cdots$. The relations of the Fourier coefficients v_n and i_n to j_n, obtained from (15) and (16), are

$$(v_n/j_n) = j\omega L/(k_n^2 - k^2), \qquad k^2 = \omega^2 LC \tag{20}$$

$$(i_n/j_n) = k_n/(k_n^2 - k^2). \tag{21}$$

The driving current at the stripline gap is

$$I_0 = \int_0^a J_0(z)\,dz = aj_0. \tag{22}$$

From these results, the stored energy in the capacitor can be calculated in terms of the coefficients (j_n), and an

input impedance can be calculated from the definition

$$Z_{in} = j4\omega(W_H - W_E)/I_0 I_0^*. \tag{23}$$

The result is

$$Z_{in} = -j\frac{Z_0}{a}\left[\frac{1}{k} + \frac{1}{4}\sum_{n=1}^{\infty} A_n^2\left(\frac{1}{k+k_n} + \frac{1}{k-k_n}\right)\right] \tag{24}$$

where $A_n^2 = |j_n/j_0|^2$.

Equation (24) has all the poles (parallel resonances) of the impedance of the open line when driven at one end, as one can see from the series representation

$$-jZ_0 \cot ka = -j\frac{Z_0}{a}\left\{\frac{1}{k} + \sum_{n=1}^{\infty}\left(\frac{1}{k+k_n} + \frac{1}{k-k_n}\right)\right\}. \tag{25}$$

In both cases, there is a zero (series resonance) between adjacent poles. The residues at the poles in (25) are all equal; as a result, zeros are always exactly midway between poles. The residues in (24) depend on the current distribution $J_0(z)$, and their values affect the locations of the interspersed zeros.

When the distribution of induced current is symmetric about $z = (a/2)$, $j_n = 0 = A_n^2$ for odd values of n. Thus, all odd ordered poles are removed, and the zeros coalesce so that there is but one zero between adjacent poles. The new zeros are close to the poles that have been removed, but they will not coincide exactly unless $A_{2n}^2 = 4$. This is the case when the induced current is an impulse function at the center. Then, (24) has the form of (25) with k_n redefined.

C. The Effects of Skin Depth on Losses

When electrode thickness is comparable to the skin depth, the fields in two adjacent regions of overlapping electrodes are not shielded from each other. The resulting coupling between transmission line periods introduces complications not contained in our proposed simple model. In particular, the losses in the electrodes will depend on the current distribution along the folded line and in the interior of each electrode. When the line is unfolded, these losses must be assigned to each period in a way that takes account of the unfolding process and the original current distribution. It is not correct simply to assign a constant resistance per meter for all sections of the developed line.

The dependence of losses on current distribution can be demonstrated with the simple capacitor illustrated in Fig. 7(a). The unfolding shown in Fig. 7(b) maintains the lengths of surfaces carrying oppositely directed currents. The essential feature is the splitting of the internal electrode to produce the two thin sections, B and C, of the developed line. In order to simplify the calculations, we assume (i) that the lengths of A and D are very small compared to the total length of B and C, and (ii) that most loss occurs in B and C.

For the current density in the z direction at a point in the cross section of the internal electrode, we write

$$J(x,z) = J_1(z)e^{-\Gamma x} + J_2(z)e^{+\Gamma x} \tag{26}$$

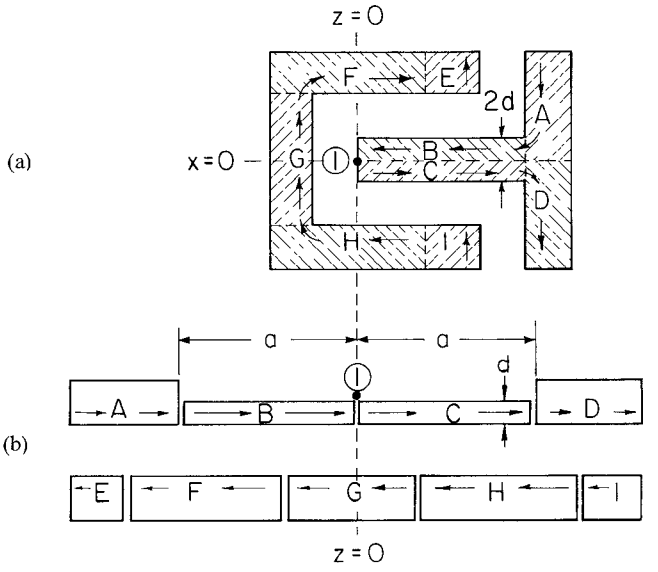

Fig. 7. Illustration of (a) the cross section of a simple capacitor and (b) its development into a parallel-plate transmission line.

where $\Gamma = (1+j)/\delta$ and δ is the skin depth. After unfolding the line, the current in section B is

$$I(-z) = w\int_0^d J(x,z)\,dx \tag{27}$$

and in section C, it is

$$I(z) = w\int_{-d}^{0} J(x,z)\,dx. \tag{28}$$

The coefficients $J_1(z)$ and $J_2(z)$ are related to the even and odd parts of $I(z)$ by the equation

$$J_{1,2} = \frac{\Gamma}{2w}\left[\frac{I_{evn}(z)}{\sinh \Gamma d} \pm \frac{I_{odd}(z)}{\cosh \Gamma d - 1}\right] \tag{29}$$

where the subscript 2 applies to the lower sign.

The power dissipated in the center electrode is

$$P = \frac{\rho w}{2}\int_0^a \int_{-d}^{d} J(x,z)J^*(x,z)\,dx\,dz \tag{30}$$

where ρ = the resistivity of the electrode. The part of the integrand that is odd with respect to x is also odd with respect to z. After the x integration, the integrand is even with respect to z, and the remaining terms can be integrated over the full developed length $(-a, a)$ to obtain

$$P = R_0\frac{1}{2a}\int_{-a}^{a}\left(D_{evn}^2|I_{evn}|^2 + D_{odd}^2|I_{odd}|^2\right)dz \tag{31}$$

where $R_0 = \rho(2a/dw)$ is the dc resistance of sections C and B and

$$D_{evn}^2 = \frac{(d/\delta)(\sinh 2d/\delta + \sin 2d/\delta)}{2|\sinh \Gamma d|^2} \tag{32}$$

$$D_{odd}^2 = \frac{(d/\delta)(\sinh 2d/\delta - \sin 2d/\delta)}{2|\cosh \Gamma d - 1|^2}. \tag{33}$$

In the limit as $\delta \to 0$ both coefficients approach (d/δ), but in the low-frequency limit $D_{evn}^2 \to 1$ while $D_{odd}^2 \to 4/3$. For a dc current, $P = R_0 I_0^2$.

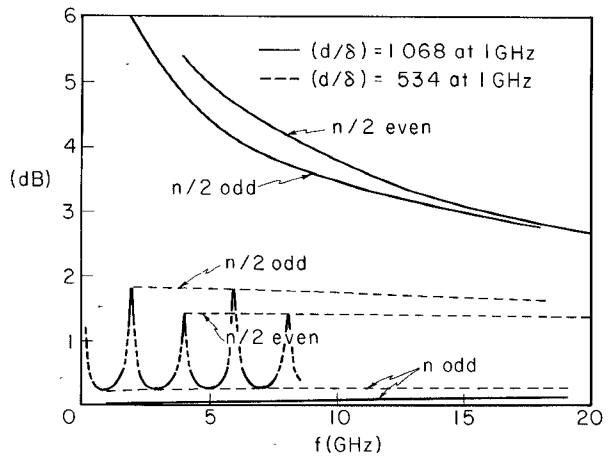

Fig 8. Envelopes of maxima and minima of the dissipation loss at resonances of the capacitor of Fig. 7.

For an open circuit at $z = a$ and a current

$$I = I_0(\sin ka \cos kz - \cos ka \sin kz) \tag{34}$$

the normalized dissipation is

$$p = \frac{2P}{I_0^2 Z_c} = \frac{R_0}{Z_c}\left\{ D_{\text{evn}}^2 \sin^2 ka\left(1 + \frac{\sin 2ka}{2ka}\right) + D_{\text{odd}}^2 \cos^2 ka\left(1 - \frac{\sin 2ka}{2ka}\right)\right\}. \tag{35}$$

At a resonance, $2ka = n(\pi/2)$; $n = 1, 2, \cdots$. Series resonances occur when n is odd, and the even values correspond to parallel resonances. The normalized dissipation at a particular value of n is designated as p_n. The input impedance at resonance is

$$Z_n = Z_c(1/p_n)^{(-1)^n}. \tag{36}$$

The corresponding dissipation loss is then

$$L_{\text{dis}} = 10 \log(1 + Z_n/Z_0). \tag{37}$$

Equation (37) is used to calculate the envelopes, shown in Fig. 8, of maxima and minima of the dissipation loss. The calculations are for $(Z_c/Z_0) = 0.160$ and a first series resonance of 1 GHz, corresponding to a capacity of approximately 30 pF. The values of the ratio of (d/δ) at 1 GHz have been chosen to demonstrate its effect on the relative amplitudes of the dissipation losses at parallel resonances with $n/2$ odd and $n/2$ even. In both cases, the envelopes cross each other. The upper two solid curves cross at some frequency less than 2 GHz, but the upper dashed curves cross at a frequency much above 20 GHz. The value of (0.534) for (d/δ) at 1 GHz is the more realistic estimate for a capacitor.

IV. Comparison of Data with Theory

The test of (7) or (9) is whether or not the measured resonant frequencies can be calculated by putting $\psi = (n/N)\pi$, $n = 1, 2, \cdots, N$, given appropriate values for η and l_1. Although these parameter values could be calculated by a numerical analysis of the field problem, the validity of the results would be compromised by unknown faults in capacitor fabrication. Since other schemes for determining η and l_1 suffer from similar limitations, the best one can expect is qualitative correspondence between data and model.

One option is to choose η and l_1 so that (7), regarded as a two-parameter function, is an optimum fit to the data. The resulting parameter values, however, may have no transparent relationship to capacitor construction, and the quality of the fit may have no relevance to the validity of the equation. Some other two-parameter function might fit as well or better.

A second approach, which has the merits of relying on experiments independent of the frequency data, is the determination of η and l_1 from the measurement of C_0 and L_0, using (11) and (12). Weighing against the procedure is the need to disect the capacitor to measure L_0 and to determine whether the value of C_0 indicates fringing capacitance or a structural fault. In the cases where the surgery has been performed, a very small fringing capacitance has been found. The inductance, which could not be measured with adequate precision, was found to be less than $\mu_0 l_2(Nt/w)$.

What appears to be the best option is to require that (7) yield the correct cutoff frequency, a quantity which may be measurable, and to drop the fringing capacitance. If we approximate the cutoff frequency by

$$f_{\text{co}} = v_{\text{ph}}/2l_2 \tag{38}$$

a relationship between η and l_2 is established.

As both parameters go to zero, thus eliminating the capacitive susceptance,

$$\pi(l_1/\eta l_2) \to [1 + \cos \pi(l_0/l_2)]/\sin \pi(l_0/l_2). \tag{39}$$

In this limit, both (7) and (13) take the form

$$\cos \psi = \cos \pi(l_0 f/l_2 f_{\text{co}}) - B\pi(l_0 f/l_2 f_{\text{co}}) \sin \pi(l_0 f/l_2 f_{\text{co}}) \tag{40}$$

where $B = [1 + \cos \pi(l_0/l_2)]/[\pi(l_0/l_2) \sin \pi(l_0/l_2)]$.

The solid curve in Fig. 9 is a plot of (f/f_{co}) versus (ψ/π) calculated from (40) with $(l_0/l_2) = (1/2)$. This value of (l_0/l_2) applies to many of the capacitors tested, and the change in the curve for other values of (l_0/l_2) is small, occurring mostly near $\psi = \pi$. The data points are parallel resonances, assumed to occur at $\psi = \pi(n/N)$. Evidently, qualitative agreement is good. The principal discrepancy appears to be the simplistic assumption of the cutoff frequency as given by (38). The data suggest that it should be higher. Moreover, (38) is equivalent to the assumption that $L_0 = \mu_0 l_2(Nt/w)$, an estimate that is high.

The suppression of odd ordered H-mounting resonances when the capacitor is in the V-mounting is qualitatively predicted by the uniform line model driven by a distributed source. The analysis of the model leads to the conjecture born out in Fig. 5(c) that full suppression of the odd ordered resonances may fail if the V-mounting is off center. The polar plot of the S_{11} of Fig. 5(c) (not included

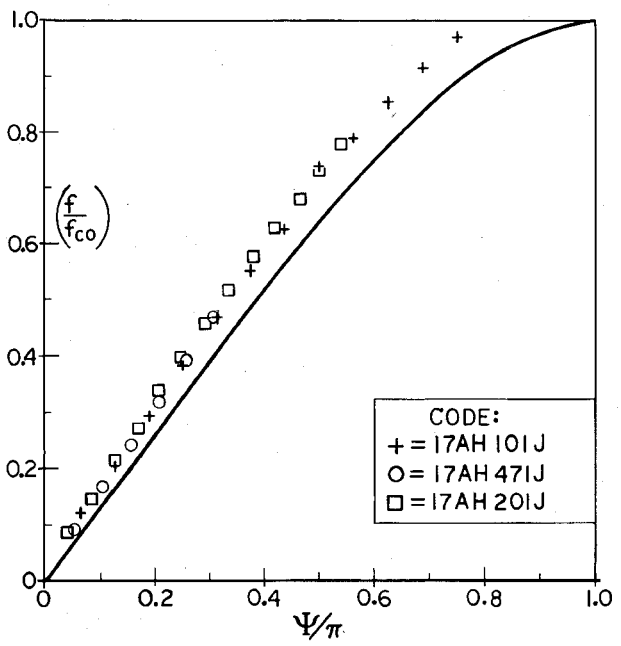

Fig. 9. Solid curve is plot of (f/f_{co}) versus (ψ/π) calculated from (40). Data points are observed parallel resonances.

here) shows two series resonances just above and below the weak parallel resonance. These data are consistent with the contention, based on the model, that two adjacent zeros coalesce as the residue at the pole approaches zero.

The simple model of Fig. 8 fails to account for the quasi-periodic characteristic of the dissipation loss at resonance, as shown in Fig. 6, but it shows that oscillations of the minima and maxima are a consequence of the folds in the line and the fact that electrode thickness and skin depth are of the same order of magnitude.

V. Concluding Remarks

The evidence that monolithic capacitors have the characteristics of folded transmission lines can be summarized as follows:

(i) Resonances occur in a sequence with diminishing frequency differences that indicate the existence of a cutoff frequency.

(ii) The dispersion equation of a simplified, periodically loaded line corresponds at least qualitatively to the observed resonances.

The suppression or occurrences of resonances as they depend on the capacitor orientation is qualitatively explained in terms of a uniform line with a distributed source.

A simple model of a folded line shows that successive maxima (and minima) of dissipation loss do not fall on smooth envelope curves. This quasi-periodicity is affected by skin depth relative to electrode thickness. Better correspondence to observed dissipation loss might be improved with a more sophisticated model.

Acknowledgment

The many contributions of D. A. Lupfer, Vice President and General Manager of Dielectric Laboratories, Inc., are gratefully recognized. Several hundred pages of data were produced by L. M. Opalko.

References

[1] V. F. Perna, *The RF Capacitor Handbook*, American Technical Ceramics, 1983, p. 2-5-17. The folded line concept is mentioned as "recently proposed," but the proposer is not identified.

[2] M. Ingalls and G. Kent, "Measurement of the characteristics of high-Q ceramic capacitors," *IEEE Trans. Components, Hybrids, Manuf. Technol.*, in press.

[3] V. F. Perna, *The RF Capacitor Handbook*, American Technical Ceramics, 1983, section 3.

[4] T. Ballarano, "Synthesis of a ladder network based on HP-8510 measurements of a 470 pF monolithic capacitor," private communication, Aug. 1985.

[5] N. Marcuvitz, *Waveguide Handbook*. New York: Dover Publications, 1951, ch. 1.

[6] D. A. Watkins, *Topics in Electromagnetic Theory*. New York: Wiley, 1958.

Mark Ingalls received the B.S. degree from Cornell University in 1977. His various careers have included dairy farming, cabinetmaking, and engineering. Employed at Dielectric Laboratories, Mr. Ingalls is also studying physics at Syracuse University. He is currently responsible for the design and construction of test fixtures used at dc, RF, and microwave frequencies, both for experimental and for production measurements. Mr. Ingalls has written software for various computer-aided test systems.

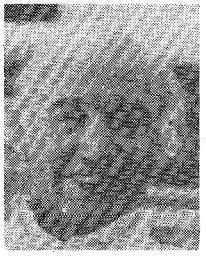

Gordon Kent (S'47–A'52–M'56–SM'73) was educated at the University of Wisconsin, Madison, (B.S.E.E.) and Stanford University (M.S.E.E. and Ph.D., 1953). While at Stanford, he worked as a Research Assistant in the Microwave Laboratory, where much of the development of the Stanford Linear Accelerator was taking place.

He was employed in 1952 as a Research Engineer by the Institute for Advanced Studies at Princeton, NJ, to work on the development of the Institute's pioneer computer. He was designated one of the "computer pioneers" by the American Federation of Information Processing Societies and the 1975 National Conference Steering Committee. From 1954 to 1957, Dr. Kent was a Research Fellow in Electronics at Harvard University. Much of his research during that period concerned a microwave oscillator that came to be known as the "Osaka tube." He was a member of the faculty at Syracuse University from 1957 until retiring in 1986.

The diverse fields in which Dr. Kent has published include numerical analysis, engineering education, solar cells, electron beams, microwave properties of plasmas, and nonlinear waves.